Environmental Toxicology
& Chemistry

Correlating Quantitative Measurements of Photocatalytic TiO_2 Radical Production to *Daphnia magna* Toxicity

Journal:	*Environmental Toxicology and Chemistry*
Manuscript ID	ETCJ-Jul-20-00557
Wiley - Manuscript type:	Original Article
Mandatory Keywords:	phototoxicity, nanoparticles, aquatic toxicology
Additional Keywords (Optional):	superoxide, Natural Organic Matter, hydroxyl radical
Abstract:	Increased use of titanium dioxide (TiO_2) nanoparticles in domestic and industrial applications has increased risk for adverse environmental outcomes based on an elevated likelihood of organism exposure. Anatase TiO_2 is photoactive with exposure to ultraviolet light. Anatase TiO_2 nanoparticle exposure to UV-A radiation in aquatic environments generates radical oxygen species (ROS), which may ultimately be responsible for increased organism toxicity. Herein we identify and measure the two most relevant ROS species, hydroxyl and superoxide radicals, and describe that these ROS can be modeled using the highly reactive hydroxyl radical to provide an upper bound for toxicity. The present research demonstrates that the overall rate of ROS production from simulated-sunlight irradiated TiO_2 nanoparticles heavily depends on exposure conditions, particularly the presence of natural organic matter (NOM). Environmentally relevant concentrations of TiO2 nanoparticles were co-exposed to increasing NOM amounts and simulated-sunlight UV-A intensities. Radical production rate was determined using fluorescence spectroscopy and positively correlated with increased TiO_2 concentration and UV-A intensity, and negatively correlated to increased DOC concentration. Nanoparticle aggregation and decreased light transmission from NOM had negligible contributions to radical production rate. This suggests decreased radical production rate is a result of quenching by NOM functionalities. *Daphnia magna* toxicity was found to decrease with NOM addition and is correlated to decreased radical production rate with increased DOC concentrations. Thus, the presence of DOC provides rate attenuation that is protective to aquatic organisms. These conclusions demonstrate the importance of considering exposure conditions during TiO_2 nanoparticle toxicity testing and during TiO_2 nanoparticle waste management and regulatory decisions.

Running Head: Quantitative measurements of photocatalytic TiO_2 radicals

CORRELATING QUANTITATIVE MEASUREMENTS OF PHOTOCATALYTIC TIO_2 RADICAL PRODUCTION TO *Daphnia magna* TOXICITY

ABSTRACT

Increased use of titanium dioxide (TiO_2) nanoparticles in domestic and industrial applications has increased risk for adverse environmental outcomes based on an elevated likelihood of organism exposure. Anatase TiO_2 is photoactive with exposure to ultraviolet light. Anatase titanium dioxide (TiO_2) nanoparticle exposure to UV-A radiation in aquatic environments generates radical oxygen species (ROS), which may ultimately be responsible for increased organism toxicity. Herein we identify and measure the two most relevant ROS species, hydroxyl and superoxide radicals, and describe that these ROS can be modeled using the highly reactive hydroxyl radical to provide an upper bound for toxicity. The present research demonstrates that the overall rate of ROS production from simulated-sunlight irradiated TiO_2 nanoparticles heavily depends on exposure conditions, particularly the presence of natural organic matter (NOM). Environmentally relevant concentrations of TiO_2 nanoparticles were co-exposed to increasing NOM amounts and simulated-sunlight UV-A intensities. Radical production rate was determined using fluorescence spectroscopy and positively correlated with increased TiO_2 concentration and UV-A intensity, and negatively correlated to increased DOC concentration. Nanoparticle aggregation and decreased light transmission from NOM had negligible contributions to radical production rate. This suggests decreased radical production rate is a result of quenching by NOM functionalities. *D. magna* toxicity was found to decrease with NOM addition and is correlated to

decreased radical production rate with increased DOC concentrations. Thus, the presence of DOC provides rate attenuation that is protective to aquatic organisms. These conclusions demonstrate the importance of considering exposure conditions during TiO_2 nanoparticle toxicity testing and during TiO_2 nanoparticle waste management and regulatory decisions.

Keywords: TiO_2 nanoparticles; superoxide; NOM; hydroxyl radical; phototoxicity

INTRODUCTION

Anatase titanium dioxide nanoparticles (TiO_2 NPs) are an active component in a multitude of industrial, personal, and everyday products. Specific uses include photocatalysts, paints, and surface coatings (Klaine et al. 2008) due to the intrinsic abilities to generate excited electrons when exposed to ultraviolet-A (UV-A) radiation. The photo-induced mechanism of electron promotion generates radical species, a property that has found application in the generation of H_2 gas, decomposition of organic molecules and persistent chemicals, and killing of bacteria and other microorganisms (Chen and Mao 2007; Gupta and Tripathi 2011). TiO_2 NP radical production may also contribute to their environmental toxicity (Ma et al. 2012a), and the small size of these nanoparticles facilitate their release into and transport through environmental compartments (Praetorius et al. 2012; Lazareva and Keller 2014). As TiO_2 nanoparticle use becomes more commonplace, it is important to understand how influential a non-target surrounding environment is on their behavior, and the subsequent risk the nanoparticles pose in a non-target setting.

Growth in use of TiO_2 NPs is such that Robichaud et al. estimates that upper bound production of TiO_2 NPs will surpass production of bulk TiO_2 by 2022. By 2025, worldwide production of TiO_2 NPs is expected to exceed 2 million metric tons per year (Robichaud et al. 2009). Lazareva et al., predicts that approximately 88,000 tons of TiO_2 NPs per year will be released (either through natural processes, disposal, or accident) to global environmental compartments (Lazareva and Keller 2014). Of this, almost 50,000 metric tons are estimated to escape wastewater treatment processes (WWTP) in the effluent, although the efficacy of removal is often dependent on the WWTP global location. WWTP with modern treatment methods are expected to sequester close to 97% of TiO_2 NPs in biosolids. However, many WWTP use

antiquated technology and the biosolids are often reutilized as fertilizer, potentially reintroducing the nanoparticles into freshwater systems (Lazareva and Keller 2014). Additional TiO_2 NP loads to water systems from surface coating/paint runoff are most likely more problematic in urban areas (Keller and Lazareva 2013). Considering predictions of exponential increases in NP manufacturing over the coming years, increasing amounts of nanoparticles can be expected to reach environmental compartments.

The movement of NPs to environmental compartments demonstrates the hazard of TiO_2 NPs to aquatic organisms. The risk presented by TiO_2 NPs can be understood when considering the photocatalytic effects of the nanoparticle. UV-A radiation at wavelengths of 382 nm has the equivalent energy of 3.2 eV; the approximate bandgap energy of anatase TiO_2 NPs. Energy of this wavelength excites electrons in the valance band, promoting them to the conductance band, and leaving behind areas of positive charges referred to as 'holes'. Electrons are transferred from water molecules to fill the holes, generating hydroxyl radical ($^{\bullet}OH$), and initiating oxidative reactions. The promoted electron also induces a reductive pathway reaction via transfer to dioxygen, generating superoxide anion ($O_2^{\bullet-}$) (Schneider et al. 2014).

Fujishima details the following reactive oxygen species (ROS) generation schemes at the TiO_2 nanoparticle surface, resulting in both surface adsorbed and free hydroxyl radical (Fujishima and Zhang 2006):

$$O_2 + 2e^- + 2H^+ \rightarrow H_2O_2 \quad (1)$$

$$O_2^{\bullet-} + O_2^{\bullet-} + 2H^+ \rightarrow H_2O_2 + O_2 \quad (2)$$

$$H_2O_2 + e^- \rightarrow {}^{\bullet}OH + OH^- \quad (3) \text{ (surface adsorbed } {}^{\bullet}OH)$$

$$H_2O_2 + O_2^{\bullet-} \rightarrow {}^{\bullet}OH + OH^- + O_2 \quad (4) \text{ (free and surface adsorbed } {}^{\bullet}OH)$$

$$H_2O_2 + h\nu \rightarrow {}^{\bullet}OH + {}^{\bullet}OH \quad (5) \text{ (free and surface adsorbed } {}^{\bullet}OH)$$

The ultimate end product of these reactions is largely hydroxyl radical. Hydroxyl is largely responsible for chemical degradation and microbial destruction, which make TiO_2 nanoparticles an attractive means for biocides and surface treatments (Gupta and Tripathi 2011). Although other ROS also are known to cause biological dysfunction through oxidative damage, hydroxyl radical exhibits the highest reduction potential of all ROS and is the most damaging (Shi et al. 2013). Because the TiO_2 nanoparticle must be activated by light, hydroxyl radical interaction with outer cellular membranes resulting in lipid peroxidation is the most common mechanism of photoactivated TiO_2 toxicity (Yin et al. 2012). Initiation of lipid peroxidation cycles resulting in membrane disruption can generate DNA adducts causing sequence mutations, and will initiate radical cycling cascades within cells (Yin et al. 2012; Fu et al. 2014; Cadet et al. 2017). It should therefore come as no surprise that these nanoparticles are toxic to non-target organisms when released into the environment (Haynes et al. 2017), largely due to hydroxyl-radical-induced damage.

Multiple researchers have investigated the toxicity of TiO_2 under UV irradiation (Amiano et al. 2012; Ma et al. 2012b; Kim et al. 2014; Mansfield et al. 2015; Lüderwald et al. 2019). These studies use natural or simulated sunlight, that appropriately reflect relevant UV intensities at the surface or shallows of freshwater bodies. Ma et al. (Ma et al. 2012a) conducted a robust battery of tests showing that the phototoxicity of TiO_2 nanoparticles to *D. magna* is partially dependent on the intensity and wavelength of UV light. Li et al. (Li et al. 2015), demonstrated that increases in UV exposure time and intensity increase TiO_2 toxicity to *Hyalella azteca*. Numerous studies indicate that the toxicity can vary by multiple orders of magnitude depending on a number of physical particle factors, such as crystal configuration (He et al. 2016), size of

nanoparticle (Wyrwoll et al. 2016), aggregation (Sharma 2009), and surface coatings (Al-Abed et al. 2016; He et al. 2016).

TiO_2 nanoparticle toxicity has been shown to follow the Bunsen-Roscoe Law of Reciprocity (Bunsen and Roscoe 1862), similar to polycyclic aromatic hydrocarbons (PAHs) (Oris and Giesy 1986; Ankley et al. 1995)**,** wherein low concentrations of TiO_2 nanoparticles and high doses of UV light produce equivalent impact compared with high concentrations of TiO_2 nanoparticles and low doses of UV light. This law can be further applied to describe the generation of photochemical products as being proportional to the product of light intensity and time (Oris and Giesy 1986; Ankley et al. 1995). Previous research has demonstrated toxicity, hypothesized to be the result of ROS, will be proportional to both nanoparticle concentration and UV intensity. (Ma et al. 2012a; Li et al. 2015; Mansfield et al. 2015; Wormington et al. 2017).

Considering TiO_2 photocatalysis in natural aquatic compartments, an important factor to consider is the effect of dissolved organic carbon (DOC) existing as natural organic matter (NOM). NOM is a significant component of natural water systems, composed of humic acids, fulvic acids, lignin, proteins, and many other organic compounds. It is ubiquitous in natural waters but the particular molecular configuration and relative concentrations vary spatially and temporally (Diem et al. 2013). Due to the persistence of NOM in water systems, it is important to determine its effects on radical generation from irradiated TiO_2.

Until recently, literature regarding TiO_2 nanoparticles did not focus on the more complex interactions that nanoparticles undergo in surface freshwaters and the resulting effect on toxicity. Studies have focused mainly on the effect of UV light and physical characteristics of the nanoparticle, such as size, crystalline configurations and coatings (Jovanović 2015). More recent work has demonstrated the necessity of incorporating NOM into studies (Wormington et al.

2017; Lüderwald et al. 2019) due to both the ubiquitous presence of NOM in all surface waters, and the inherent ability of organic compounds such as NOM to quench radical species (Haynes et al. 2017). Identifying the influences of changing environmental conditions on the TiO_2 nanoparticle will help to develop a better understanding of the link between ROS generation and thus TiO_2 toxicity. Further, the photocatalytic effects of TiO_2 nanoparticles can be leveraged for water treatment and breakdown of humic substances, since photocatalytic TiO_2-enhanced treatment can remove up to 80% of DOC (Uyguner and Bekbolet 2005; Liu et al. 2010; Drosos et al. 2015), and TiO_2 nanoparticles have been used as a method to reduce filter biofouling (Huang et al. 2008). Understanding the dynamic interactions may add insight to creating more efficient water treatment systems.

Our study combines relevant concentrations of TiO_2 nanoparticles, a novel element of simulated-sunlight conditions approximating those deeper within the photic zone, and relevant concentrations of Suwanee River water NOM. Our goals are to 1) identify the radical species produced under these conditions, 2) provide a more direct model of TiO_2 phototoxicity, by quantitatively linking parameters influencing radical generation to changes in overall production, and 3) link these quantitative changes to toxicity outcomes. By defining a radical species to use as a toxicological model, we can enhance approximations of toxicity, considering known radical behavior. By bounding experiments at reasonable environmental concentrations of TiO_2 and NOM, and light intensities, more accurate predictions about the behavior of TiO_2 NPs outside of a laboratory setting can be made. By incorporating relevant values of these parameters via a full factorial interaction, we can achieve a more discrete understanding of subtle variations in TiO_2/environment/organism dynamics. Based on previous literature, we hypothesize that

variations in TiO_2 concentration, light intensity, and NOM amounts can be correlated with ROS production radical generation, which invariably influences environmental toxicity.

MATERIALS AND METHODS

Full Factorial Design

A full factorial approach to exposures was used for this experiment. The TiO_2 NP concentrations tested were 0.0, 0.50, 1.00, 3.50, 5.00, 7.00, 10.5, and 14.0 mg/L. Dissolved organic carbon (DOC) concentrations were 0.00, 1.57, 2.95, 4.28, and 5.71 mg/L. UV intensities were measured as irradiant intensity per nm, averaged across 320-400 nm, and were 0.00, 2.67, 4.30, and 5.17 $\mu W/cm^2/nm$.

Titanium Dioxide Nanoparticle Suspensions

Anatase titanium dioxide nanoparticles (Aldrich, <25-nm, 99.7% metals basis) were suspended in 18 mega-Ohm water, at a concentration no greater than 100 mg/L. Upon the initial dispersion into stock suspensions, TiO_2 NPs were stirred for 10 min and sonicated for 2 h (in 15 min on/5 min off intervals) using an immersion-tip sonicator. Before use, stock suspension was sonicated for 15 min, and lightly stirred during dilutions to ensure complete suspension. All suspensions were diluted with EPA recipe Moderately Hard Water (MHW) (96.0 mg/L $NaSO_4$, 60 mg/L $CaSO_4$-H_2O, 60 mg/L $MgSO_2$, 4.0 mg/L KCl; pH: 7.9-8.3; hardness: 80-100, alkalinity: 57-64) (USEPA 2006).

Nanoparticle size distributions were measured using Hitachi H7600 TEM. Intensity weighted hydrodynamic diameter was determined by DLS using a Wyatt Dawn Heleos-II, at ambient temperature. UV transmission was determined, using a Varian Cary 50 Bio UV-Vis spectrophotometer, analyzed from 300 to 700 nm at a scan rate of 100 nm/min, with 1 nm

intervals. Aliquots of 0.5 mL were analyzed using quartz 1 cm × 1 cm × 4.5 cm plastic cuvettes (Spectrasil), at room temperature. Zeta potential was measured using a Malvern Zetasizer ZS, at room temperature. DLS and UV transmission were run for the full factorial of TiO_2, DOC concentrations and UV intensities, measured at 0, 24, and 48 h. Zeta potential was only determined at initial time of preparation, for the full factorial of DOC and TiO_2.

Natural Organic Matter

Natural organic matter was obtained directly from the Suwannee River headwaters, at Suwannee River Visitors Center in Fargo, Georgia**.** Water was filtered through 0.45 micron filters to remove all non-dissolved components. Filtered Suwannee River water was lyophilized to determine the total amount of dissolved organic matter (DOM) per liter. Total organic carbon concentration was determined using a Shimadzu TOC-V Carbon Analyzer. Stock concentrations were directly diluted in EPA recipe MHW to achieve working concentrations.

Light System

UV irradiance was generated using CXL Topaz 40W Blacklight Blue T-12 Fluorescent lights. Standard Lab lighting was generated using Sylvania 40W Cool White T-12 Fluorescent lights. Lights were installed in a plywood light box, measuring 48” × 12” × 12.5”, with an 8” distance from bulb to bench surface. Intensity and spectral output were measured using an OceanOptics JAZ Photospectrometer equipped with a cosine corrector. Spectroscopic data was analyzed using OceanView 1.5.2.

Electron Paramagnetic Resonance Spectroscopy

EPR spectroscopy was used to identify radicals produced from the irradiation of TiO_2 NP suspension. X-band EPR measurements were acquired using a Bruker EMX spectrometer, with a quartz flat cell inserted directly into the microwave cavity at ambient temperature. For all

experiments, the following parameters apply: modulation frequency and amplitude were 100 kHz and 0.5 G, microwave frequency was 9.759 GHz, microwave power was 1.00 mW. Time constant and conversion time equaled 81.92. Sweep width was 100 G centered at 3479 G. The g-factor of 2,2,-diphenyl-1-pierylhydrazyl (DPPH; g = 2.0036) was used as an external reference. Spectra were analyzed using WIN EPR software.

5,5-Dimethyl-1-pyrroline-N-oxide (DMPO) was used as a spin trap for both standards and samples. Copper sulfate/ascorbic acid/hydrogen peroxide standards were used to verify the EPR DMPO-hydroxyl-radical adduct signature. $CuSO_4$ (15 µL, 300 µM), ascorbic acid (9.38 µL, 375 µM), 3-morpholinopropane-sulfonic acid (MOPS) buffer (50 µL, 10 µM), H_2O_2 (11.25 µL, 22.5 µM), and ultra-pure deionized water (414.38 µL) were combined in a microcentrifuge tube and mixed. DMPO (25 µL, 25 mM) was immediately added, mixed, and the solution was transferred to the quartz flat cell and immediately inserted into the EPR microwave cavity.

TiO_2 NP suspensions were made in 50 mL volumetric flasks and separated into triplicate scintillation vials of 15 mL per vial and covered with UV transparent Aclar® film. Samples were irradiated under CLX black lights for 48 h, with analysis points at 0, 24, and 48 h. At each time point, DMPO was added, and the vials were removed from the UV box. Aliquots of 0.5 mL for each sample were taken, added to the quartz flat-cell, and immediately inserted into the microwave cavity for analysis. All EPR measurements were taken within 5 min of sample preparation.

Fluorescence Spectroscopy

Fluorescence spectroscopy was used to measure the concentration of radical species produced in each sample at each timepoint. Fluorescein dye was prepared by dissolving 0.047 g HEPES buffer (Alfa Aesar, 99%) into 10 mL ultrapure DI water in a scintillation vial. 500 µL of

10 M KOH (Acros, 85%) was added and stirred. 0.0367 g of fluorescein, free acid (Sigma) was added and stirred until complete dissolution occurred. The solution was acidified with 130 µL HNO_3 (BDH, 69%) and adjusted to pH 7.5. Final stock concentration was 100 mM. Working concentration did not exceed 7.5 µM. Sample dye concentrations were varied depending on the range of ROS generation.

Fluorescence analysis was performed on a Horiba Fluoromax-4 fluorescence spectrometer. Excitation was measured at 467 nm and emission intensity was measured from 400 to 700 nm. Excitation slit width was 1.0 nm; emission slit width was dependent on initial concentration of fluorophore.

Calibration curves to hydroxyl radical production were generated using horseradish peroxidase and hydrogen peroxide, as per the Hydroxyl Radical Antioxidant Capacity (HORAC) assay (Ou et al. 2002). 5 mg of horseradish peroxidase (HRP) (Sigma, lyophilized powder, AU: 310 units/L) was dissolved in 5 mL of 18 mega-Ohm DI water to give solution of 310 AU/L. Hydrogen peroxide (BDH, 30%) concentrations (0 to 10 µM) were combined with 107.6-µL of HRP solution, 150 µL of 1M potassium phosphate buffer (BDH, 98%) and requisite amount of fluorescein. Solutions were then diluted to 3 mL. Separate calibration curves were made for each dye concentration, with new calibration curves made for each new stock solution. To determine concentration (µM) of hydroxyl radical at a given emission, the concentration of H_2O_2 is multiplied by two, as horseradish peroxidase generates two equivalents of hydroxyl radical from one equivalent of hydrogen peroxide (Ou et al. 2002). Calibration curves are shown in the **Supplemental Information.**

All sample solutions were made in 100 mL volumetric flasks. TiO_2 NP suspensions were diluted to testing volume (0, 0.500, 1.00, 3.50, 5.00, 7.00, 10.5, or 14.0 mg/L) along with DOC

(0.00, 1.57, 2.95, 4.28, 5.71 mg/L) and fluorescein dye (1.50, 5.00, 7.50, 10.0 μM/L); 30 mL was dispensed into beakers, in triplicate. A 3 mL aliquot was removed from each for analysis, and these suspensions were immediately covered with Aclar ® Fluoropolymer film, a UV transparent film, and placed in the lightbox. Dark control 0 $\mu W/cm^2/nm$ samples were additionally covered with aluminum foil to ensure the complete blockage of UV irradiation. The samples were only removed to take 3 mL aliquots for analysis every 12 h.

Hydroxyl radical generation was determined by measuring the difference in emission from time zero. All experiments were run in triplicate, and data provided represent averages of triplicate trials. Rates were determined from the slope of a linear regression line for each concentration across 48 h. Samples with 0 mg/L TiO_2 NP concentrations were treated as a blank, and generation rates were subtracted to account for decreases in emission not related to ROS generation.

Daphnia magna *Bioassays*

Daphnia magna 48-hour acute toxicity bioassays were performed in accordance to EPA protocol and standards (United States Environmental Response Team 1991). Less than 24-hour-old neonates were randomly selected from a pool of 500 neonates raised from a multigenerational lab culture. Neonates were transferred to freshly prepared suspensions (prepared as described above). Suspension exposed to UV light (4.301 $\mu W/cm^2/nm$) ranged from 0 mg/L to 1.5 mg/L TiO_2 NP with no DOC and suspensions with 4.28 mg/L DOC ranged from 0 mg/L to 14 mg/L TiO_2. Suspensions exposed to fluorescent lab light (0.0423 $\mu W/cm^2/nm$) ranged from 0 mg/L to 1500 mg/L TiO_2 NP. All exposure vessels contained 20 mL of suspension and 5 *D. magna.* Each concentration had 3 biological replicates. Mortality was assessed and recorded at 0, 24, and 48 h. Standard 16 h light/8 h dark cycles were used, and all exposure

vessels kept at 22.5 ± 1°C. Water quality was assessed at the onset and outset of each experiment and stayed within EPA acceptable testing values. Bioassay data is described as LC50 values and were calculated for all TiO_2 NP concentrations and radical dose using standard Spearman-Karber methodology.

Statistical Analysis

All statistical analysis was performed using JMP software (version 12.1.0). Residuals confirmed for normativity using the Sharpiro-Wilk test. Comparative analysis of group means was performed using analysis of variance (ANOVA), with Tukey-Wagner HSD utilized as a *post hoc* analysis for all treatments demonstrating statistically significant differences between levels. Comparative analysis was performed on all rate data using a comparative analysis of means with a Sidak adjustment, and Tukey's HSD to determine significant differences between rates (α = 0.05). These data can be found in the **Supplemental Information.**

RESULTS and DISCUSSION

Suspension Characterization

The TiO_2 nanoparticles used in this experiment were anatase-crystal, industrial grade nanoparticles with a wide size distribution range. Using these nanoparticles allowed us to model nanoparticles that would theoretically be released into the environment post use and selecting a more photoactive form (anatase) allowed us to maximize nanoparticle radical production. TEM-measured primary particle size was 21 ± 19 nm. The greatest distribution density of nanoparticles was 14 nm. A histogram describing nanoparticle size distribution can be found in the **Supplemental Information.** The measured size conforms to product specifications, and aligns well with TiO_2 nanoparticles used in similar experiments (Ma et al. 2012b; Li et al. 2016).

No surface charge trends were evident across the TiO_2 NP gradient at any DOC concentration, nor across the DOC gradient at any one TiO_2 NP concentration. Zeta potential ranged from ~11 to ~20 mV (data are provided in the **Supplemental Information**). Our data did not indicate consistent or pattern-based significant changes to surface charge, as measured by zeta potential, so steric repulsion is most likely driving suspension stability dynamics (Liu et al. 2008; Loosli et al. 2013).

Dynamic Light Scattering (DLS) was utilized to determine whether the NP size changed over time, which could influence suspension dynamics. The z-average hydrodynamic diameter of the aggregates increased in size as TiO_2 NP and DOC concentrations were increased. Initial aggregate measurements ranged from 60 nm to 470 nm, 24 h measurements ranged from 28 nm to 623 nm, and 48 h size measurements ranged from 5 nm to 454 nm, demonstrating relatively consistent sizes over exposure time. Increases in light intensity resulted in decreases in z-average diameter particularly at the highest light intensities (5.18 $\mu W/cm^2/nm$) with the lowest concentrations of TiO_2 NPs (data provided in the **Supplemental information**).

DOM in solution as determined by triplicate measurements of lyophilized Suwanee River Water was determined to be at a concentration of 107 (± 20) mg/L. Dissolved organic carbon was determined to be 61 mg/L by TOC analysis. HPLC-ICP determined metal content is provided in the **Supplemental Information.**

The variation of aggregate sizes can be attributed to the multiplicity of interactions occurring between the TiO_2 NPs, natural organic matter, and irradiation over time. Increases in TiO_2 NP concentration result in larger aggregates, a result of charged surface interactions of the nanoparticle (Keller et al. 2010; Loosli et al. 2013). These larger aggregates experience gravimetric settling over time, resulting in removal from the water column (Mansfield et al.

2015). Loosli et al. investigated the effects of humic acid (a component of NOM) on nanoparticle colloidal stability demonstrating a maximum aggregation size occurring at 2.0-3.0 mg/L humic acid, and rapid size decrease at concentrations above 3.0 mg/L(Loosli et al. 2013). It should be noted that this was not examined in the presence of ultraviolet irradiation. NOM coated nanoparticles will experience enhanced surface charge and steric repulsion, as NOM provides negative charge and increases the colloidal stability of nanoparticles in solution (Wormington et al. 2017). Advanced photooxidation of these functionalities can modify surface charge, and influence steric interactions over time, which although outside the scope of this research, is an important aspect to consider.

Overall, we found a high degree of size polydispersity, contributed from NOM molecules of varying identities and sizes, nanoparticle aggregates, and buffer salts. This results would be similar to that in a natural water body, given the not negligible temporal and spatial variations in water body conditions that ultimately influence NP behavior (Williamson et al. 1996; Barron et al. 2008). To our knowledge, this is the first photoactive TiO_2 study that has directly used Suwanee River water, as opposed to singular NOM constituents (Loosli et al. 2013) reconstituted Suwanee River water Organic Matter (SROM) (Li et al. 2016; Wormington et al. 2017), or alginate (Lüderwald et al. 2019), which adds an enhanced degree of analogy to real-world conditions. The complexity of these suspensions demonstrate the multiplicity of interactions TiO_2 nanoparticles undergo in an aquatic environment and demonstrate the need for further investigation.

Light Characterization

Light intensities generated by CLX black lights in the UV-A range (320-400 nm) measured between 2.67 to 5.18 $\mu W/cm^2/nm$, with peak intensity occurring at 365 nm. Lighting

characterization can be found in the **Supplemental Information** section. The UV-Vis percent transmission spectra were examined to measure light impedance as a result of increasing DOC. Within the working range of the experiment (0 to 5.71 mg/L DOC), the increases in DOC concentration result in a maximum of a 10% transmission decrease. These data are summarized in the **Supplemental Information**. Our light intensities are comparable to those found in natural water bodies (Williamson et al. 1996) and also to intensities used in similar studies (Li et al. 2016; Wormington et al. 2017). These light intensities can be compared to the measured intensity of sunlight at noon in August in Pendleton, South Carolina (34.6518°N, 82.7838°W), 45.08 $\mu W/cm^2$ (data not shown). The transmission results agree with Wormington et al., who demonstrated that similar decreases in percent transmission do not impact the hydroxyl radical production rate (Wormington et al. 2017).

Identification of Reactive Oxygen Species (ROS)

Because radicals are so short lived, few analytical techniques can directly identify them. EPR is a technique able to characterize radicals by forcing electrons to align to an energy field and then energetically promoting them to higher energy levels with a combination of microwave radiation and magnetic field modulation. The movement of electrons from one energy level to another generates a distinct, identifiable spectrum for individual radical species (J.N.Junk 2012). A more detailed explanation of this technique can be found in the **Supporting Information**. However, due to the extremely short lifetime of most oxygen-based radicals, 'spin-traps' are utilized to create more stable radical adducts. Nitrone-containing spin-traps, such as DMSO, are commonly employed in TiO_2 radical studies. We chose DMPO as our spin trap, as it detects multiple radical species known to be generated by irradiated TiO_2 (Shibata et al. 1998; Li et al.

2014). Identifying all the ROS generated was critical to both understanding biological implications and for selecting an appropriate dye for radical quantification.

A standard spectrum generated with copper sulfate/ascorbic acid/hydrogen peroxide (**Figure 1A**) was compared to spectra from the irradiated TiO_2 NP sample (**Figure 1B**). The hydroxyl radical adduct, DMPO-$^{\bullet}$OH, generates a clear 1:2:2:1 quartet, plainly recognizable in the $CuSO_4$/citric acid/H_2O_2 standard spectrum (**Figure 1A)**. EPR spectra from the irradiated TiO_2 suspension (**Figure 1B)** indicated formation of a number of radical species. Resonances derived from DMPO-$^{\bullet}$OH generation are highlighted in green. The superoxide radical-adduct (DMPO-$O_2^{\bullet-}$, highlighted in yellow) and nitroxide-like radicals (starred), were also found and confirmed by comparison to reported spectra (Diaz-Uribe et al. 2010). These radical species identified from irradiated TiO_2 NPs were comparable to irradiated TiO_2 NPs spectra published by several groups (Brezová et al. 2007; Miller et al. 2012; Dvoranová et al. 2014), suggesting that radical formation upon simulated sunlight irradiation is comparable to laser irradiation (Brezová et al. 2007; Dvoranová et al. 2014), despite a significantly lower radiation intensity and a broader wavelength spectrum.

The nitroxide-like radical signature indicated with asterisks in **Figure 1B** was previously identified as a light-induced-decomposition product of DMPO-$O_2^{\bullet-}$, formed from N-C bond cleavage and ring opening of the DMPO-$O_2^{\bullet-}$ adduct (Bosnjakovic and Schlick 2006; Diaz-Uribe et al. 2010). This nitroxide-like radical would not form in the absence of DMPO and therefore the two ROS products generated by TiO_2 NP irradiation are hydroxyl and superoxide radical. This result agrees with reports that TiO_2 NP irradiation (halogen lamp (Diaz-Uribe et al. 2010); UV-emitting lamps (Miller et al. 2012)) primarily produces $O_2^{\bullet-}$ and $^{\bullet}$OH, as well as

singlet oxygen (Konaka et al. 2001), $^1O_2$. $^1O_2$ was not detected in our suspensions as it does not react with DMPO (Konaka et al. 2001).

Measurement of ROS Generation Rates

EPR spectroscopic methods can unambiguously establish the presence of specific radical species, but this method provides only a 'snap-shot' in time. Long-term radical quantitation studies were also conducted using fluorescence spectroscopy techniques. Fluorescein has previously been used to quantify radicals generated by irradiated TiO_2 NPs (Wormington et al. 2017). Fluorescein dyes are susceptible to oxidation and will react with ROS species to form resonance moieties of varying fluorescent intensity. This is highly dependent on substituent groups attached to the main fluorescent core (Wardman 2007). Indeed, there are many probes that react with specific ROS (e.g. bis(diphenylphosphinyl)fluorescein for $O_2^{\bullet-}$, hydroxyphenol fluorescein or aminophenyl fluorescein for $^{\bullet}OH$) (Newton and Milligan 2006; Scientific 2010), however we have established via our EPR studies that both $O_2^{\bullet-}$ and $^{\bullet}OH$ are generated, so both must be accounted for. The fluorescein dye used in this experiment has the ability to react with both $O_2^{\bullet-}$ and $^{\bullet}OH$ (Gomes et al. 2005), as well as singlet oxygen(Gaigalas et al. 2004) wherein the bright fluorescence of fluorescein is quenched by generated ROS, via oxidation of the molecule's benzene rings (Newton and Milligan 2006). The products resulting in the observed decrease in fluorescence emission are the same regardless of the ROS that generates them, as evidenced by lack of shoulders or additional peaks in emission spectra. Therefore, we calibrated to $^{\bullet}OH$ to account for either $O_2^{\bullet-}$ or $^{\bullet}OH$ generation using a model was based on the Hydroxyl Radical Adverting Capacity (HORAC) assay (Ou et al. 2002). Using this calibration method, we

effectively developed regression curves to directly quantify the amount of ROS generated by irradiated TiO_2 nanoparticles.

Photocatalytic ROS generation rate measurements by fluorescence (**Figure 2**) showed significant differences for TiO_2 nanoparticle suspensions with varied DOC concentrations up to ~6 mg/L, UV irradiation up to 5.18 $\mu W/cm^2/nm$, and TiO_2 NP concentration up to 14 mg/L. All ROS generation by TiO_2 NP over 48 h were observed to be linear. Generation followed distinct trends, where radical concentration increased with increasing TiO_2 NP concentration and UV intensity. Addition of DOC decreased the total amount of radicals accumulated. Reciprocity was demonstrated, where lower concentrations of TiO_2 NP and high intensities of UV light generated similar ROS concentrations compared to high TiO_2 NP concentrations and low UV intensities. All samples exposed to 0 $\mu W/cm^2/nm$ generated zero, or extremely close to zero, ROS. The calculated rates are expressed graphically in **Figure 2A** to **2D** (statistical summaries can be found in the **Supplemental Information**).

Radical generation was the greatest with the highest TiO_2 concentrations (14 mg/L) with 0 mg/L DOC, under higher UV-A light intensities. These exposures consistently generated such a high concentration of ROS that the fluorescent dye used to measure their generation was routinely diminished around the 36 h mark, so increased concentrations of dye were required at the onset of these experiments. Increased NP concentrations allow for increased photon/nanoparticle interaction, resulting in an increased rate of radical generation. These results agree with expected dependence of radical rate on TiO_2 concentration (Knorr et al. 2008; Schneider et al. 2014). Generation rate increases as light intensity increases due to an increase in photons impinging on the nanoparticle surface. This reaction generates more electron-hole pairs, ultimately resulting in an increase in ROS generation (Uchino et al. 2002; Fujishima et al. 2008;

Ma et al. 2012a; Li et al. 2015). Thus, increased rates of ROS generation from TiO_2 irradiation occurring in upper levels of the water exposed to higher UV intensities should therefore be expected. The low light intensities in this study are representative of relevant water column depths (2-10 m) (Forman et al. 2015). The significance of the radical generation at these low intensities should not be understated. Our study directly measures radical rates at conditions found non-surface areas of the water column, as opposed to surface-equivalent light intensities.

Reduction in ROS generation with the addition of NOM may be explained through three different scenarios: changes to particle surface charge resulting in changes in particle presence within the irradiated water column, reduction of light transmission due to increased NOM content, or quenching of ROS by NOM functional groups. TiO_2 NPs will aggregate, and settle over time, with quicker settling times dependent on concentration of nanoparticles, TOC concentration, and ionic strength (IS) conditions. Keller et al. measured settling rates of multiple TiO_2 NP concentrations and found that concentrations less than 10 mg/L, in waters with low ionic strength and higher TOC concentrations, were stable in suspension (~300 nm) and remained in the water column for prolonged periods. However, in waters of low TOC and high IS (such as seawater), aggregation and settling occurred rapidly (Keller et al. 2010). In this work, a majority of the nanoparticle concentrations were below 10 mg/L, the aggregates were generally around or below 300 nm in diameter with few exceptions (see **Supplemental Information**), and our solutions were made in the equivalent of freshwater. Thus, lack of suspension stability is not expected to impact ROS generation rate in our studies (Brunelli et al. 2013; Forman et al. 2015).

UV-A is attenuated by DOC, with a hyperbolic inflection point occurring at 1-2 mg/L DOC (Williamson 1996). In waters of less than 2 mg/L of DOC, UV-A has a 1% attenuation depth (the depth at which 1% of surface irradiation will penetrate) of 2 to 12 m (Williamson et

al. 1996; Liu et al. 2010). The present research has demonstrated that UV-A irradiation is maximally attenuated at 10% for the highest concentration of DOC. This 10% decrease in attenuation does not account for the large decrease in ROS rate generation, and therefore is not solely responsible for the overall ROS generation rate reduction. These results agree with previous research, demonstrating that minimal light attenuation would not cause significant decreases in generation rate (Li et al. 2016; Wormington et al. 2017).

This leaves the third possibility, that radical quenching by NOM functionalities is responsible for the decrease in measurable radical concentration. This interaction between the generated radicals and NOM functionalities is demonstrated by the breakdown of humic acids and other NOM components (Uyguner and Bekbolet 2005; Liu et al. 2010; Drosos et al. 2015). Radical reactions with phenolic chemicals is well quantified, and occur by precisely the reaction mechanism radicals undergo to react with fluorescent dyes (Cohn et al. 2008). Hydroxyl radical species react in three mechanisms of action: electron abstraction, hydrogen abstraction, and double bond addition(Turchi and Ollis 1990). Similarly, superoxide radical species react via proton abstraction, disproportionation, nucleophilic substitution, and one-electron transfer reactions (Hayyan et al. 2016). These reactions target electron rich sites of molecules, such as aromatic rings, aliphatic carbon chains (such as polyunsaturated fatty acids) or on hydroxyl or thiol functional groups (Collin 2019). Some of the most effective antioxidants are polyphenols, and increasing polyphenol concentration increases antioxidant efficiency of solutions (Číž et al. 2010). Polyphenols include hydrolyzable tannins, lignins, flavonoids, and condensed tannins. NOM is well characterized to have a wealth of these substituent groups (Pelekani et al. 1999a; Pelekani et al. 1999b). In fact, advanced oxidative processes (UV/TiO_2, O_3/H_2O_2, H_2O_2/catalysts)

that use ROS to break down NOM are already utilized in wastewater treatment plants around the world (Wang et al. 2000; Goslan et al. 2006; Matilainen and Sillanpää 2010).

Establishing trends in ROS generation from irradiated TiO_2 NPs is necessary to better describing the behavior of these NPs in complex environmental compartments. A critical component of this description includes toxicity estimations. To simplify the overall predictions, we propose describing all ROS species as a single radical species of known effects, such as the hydroxyl radical. By describing all ROS as the more biologically destructive radical, upper-bound models for toxicity can be constructed, aligning with EPA recommendations for Theoretical Upper Bound Exposure (TUBE) modeling (National Research Council 1994), and general EPA guidance on conservative estimations when calculating risk (John R. Fowle III and Dearfield 2006).

Toxicity Modeling Based on Hydroxyl Radical

ROS generation by TiO_2 NP may be simplified as hydroxyl radical for modeling purposes, as supported by a number of reasonable arguments. Although $O_2^{\bullet -}$ produced in these photocatalytic reactions have higher quantum yields than $^{\bullet}OH$ formation (Hirakawa and Nosaka 2002; Zhang and Nosaka 2013), $O_2^{\bullet -}$readily reacts with water to form H_2O_2 (Equation 2). H_2O_2 then rapidly reacts with free electrons (Equation 3), $O_2^{\bullet -}$ (Equation 4), or with light (Equation 5) to generate $^{\bullet}OH$ (Rao et al. 1980; Harbour et al. 1985; Ishibashi et al. 2000; Brezová et al. 2007; Fujishima et al. 2008; Zhang and Nosaka 2013; Schneider et al. 2014). In addition, organic intermediates in reactions photocatalyzed by irradiated TiO_2 are comparable to intermediates produced by reactions with known $^{\bullet}OH$ sources (Turchi and Ollis 1990; Nosaka et al. 2003), providing substantial evidence that $^{\bullet}OH$ is the main species involved in photocatalytic TiO_2 reactions.

Further observations of photocatalytic reactions using irradiated TiO_2 run in water-free, aerated organic solvents show significant decrease in oxidation rates of organic molecules compared to reactions run in water (Turchi and Ollis 1990). Cunningham and Srijaranai (1988), established a H_2O/D_2O kinetic isotope effect in photocatalyzed oxidation of isopropanol in an aqueous TiO_2 slurry. Replacing hydrogen with deuterium in isopropanol, while retaining hydrogen in the aqueous portion of the slurry showed no reduction in isopropanol degradation rate. However, replacing hydrogen with deuterium in the aqueous solvent reduced the reaction rate. These results confirm that the formation of active oxygen species ($^{\bullet}OH$ or $^{\bullet}OD$) from the aqueous solvent is a rate limiting step, driven by higher energy requirements of O-D bonds due to lower ground state energies compared to O-H bonds (Cunningham and Srijaranai 1988). $^1O_2$ generated by TiO_2 NP occurs by reaction of superoxide with trapped holes on the nanoparticle surface (Fujishima et al. 2008; Yin et al. 2012). However the significantly longer half-life of $^1O_2$ (10^{-6} s) (Phaniendra et al. 2015) compared to $^{\bullet}OH$ (10^{-10} s) (Phaniendra et al. 2015), makes this species less relevant for comparative oxidation reactions (Fujishima et al. 2008).

Toxicologically, although both $O_2^{\bullet-}$ and $^{\bullet}OH$ are capable of inducing cellular oxidative degradation effects, $O_2^{\bullet-}$ is both less reactive than $^{\bullet}OH$ due to its 10,000-fold longer half-life and generally poorer biological reactivity than $^{\bullet}OH$ as observed from its comparatively lower rate constant value (10^2 and 10^{10} $L \bullet mol^{-1} \bullet s^{-1}$, respectively) (Collin 2019). Superoxide also reacts quickly with superoxide dismutase (Collin 2019) to generate hydrogen peroxide that can then react with free electrons, with iron via Fenton cycling, or with another $O_2^{\bullet-}$ to generate additional $^{\bullet}OH$ (Fu et al. 2014; Cadet et al. 2017). Additionally, $O_2^{\bullet-}$ is responsible for initiating cellular response cascades, generating $^{\bullet}OH$ in the process (Fu et al. 2014). Comparatively, $^{\bullet}OH$ has no known enzymatic scavengers, and it interacts readily with biomolecules, nucleic acids, and

cellular lipid layers, resulting in adduct formation and oxidation (Evans et al. 2004; Fu et al. 2014; Cadet et al. 2017).

Implications of Modeling ROS as Hydroxyl Radical

We have demonstrated both superoxide and hydroxyl radical species are generated from the sunlight-like irradiation of TiO_2 NPs using EPR spectroscopy. This is an important distinction we make compared to recently published literature (Ma et al. 2012a; Wormington et al. 2017; Lüderwald et al. 2019), which uses sourced information on radical generation rather than direct confirmation, possibly resulting in an underestimation of total radical species produced. Herein, we make two implicit assumptions given the numerous mechanisms of $^{\bullet}OH$ generation, the wealth of data indicating $^{\bullet}OH$ is significantly more reactive than other ROS produced by irradiated TiO_2 NPs, and the known biological implications of $^{\bullet}OH$ damage. First, the superoxide radical will decompose to hydroxyl radical via a variety of chemical and biological pathways. Second, $^{\bullet}OH$ is significantly more biologically damaging compared to superoxide, making this species the most concerning of the two.

Therefore, characterizing total radical generation of irradiated TiO_2 NPs as $^{\bullet}OH$ may be an appropriate step to simplify its environmental damage potential in subsequent models. Previous studies assuming that $^{\bullet}OH$ is the sole radical species generated and only measuring that species may be underestimating the total amount of ROS generated, as we demonstrated the superoxide radical must be accounted for, and thus included when quantifying ROS. Measuring total ROS but describing the ROS entirely as $^{\bullet}OH$ therefore provides an upper bound measurement of $^{\bullet}OH$ generated by sunlight-like irradiation of TiO_2 NPs. Using this reasoning, we can discard toxicity descriptions based on NP concentration, and more accurately describe toxicity using $^{\bullet}OH$ radical concentrations. Although TiO_2 NPs are the vector for toxicity, the

ultimate toxicant is ROS (generalized here as •OH). Therefore, toxic response should be described as a function of such.

Daphnia magna *48 h Acute Bioassays*

Using EPA standard 48 h acute bioassays, we assessed the *D. magna* toxicity response to •OH, generated from simulated sunlight-irradiated TiO_2 NPs under a variety of realistic conditions. **Figure 3** shows that *Daphnia magna* mortality was well correlated with increasing TiO_2 NP concentration and UV intensity. *D. magna* exposure to TiO_2 NPs under fluorescent lighting (0.043 μW/cm^2/nm UV intensity) resulted in LC50 toxicity of 837 (675, 1370) mg/L TiO_2 NP. Exposure to UV light at a wavelength of 320-400 nm and an intensity of 4.301 μW/cm^2/nm resulted in nearly four orders of magnitude increased toxicity, with an LC50, 0.156 (0.121, 0.199) mg/LTiO_2 NP. Significant reduction occurs with addition of 4.28 mg/L DOC to suspensions exposed to UV light resulting in *D. magna* LC50 toxicity of 9.10 (8.37, 9.89) mg/L TiO_2 NP.

Figure 4 shows toxicity with UV (4.30 μW/cm^2/nm) exposure as a function of generated hydroxyl radical. Exposures with 0 mg/L DOC demonstrated much lower •OH LC50 toxicity (0.458 (0.415, 0.503) μM •OH) than in the presence of with 4.28 mg/L DOC (6.22 (5.77, 6.69) μM •OH). No •OH was generated under ambient light conditions; thus, the data are not included. Exposures without NOM had a rapid increase in toxicity per μM •OH, resulting in LC50 mortality at 0.451 μM •OH DOC presence results in a decrease of toxicity to 6.5 μM •OH. At the LC50, the rate of •OH generation for 4.28 mg/L DOC is ~ 0.203 μM/h, while at 0 mg/L DOC, the rate is ~0.014 μM/h.

We show that the rate difference results in much more TiO_2 NPs needed to produce a toxic effect in suspensions with DOC. The toxic effect therefore appears to be a result of the rate of •OH generation overwhelming the organism. In exposures with DOC, more •OH are required to cause equivalent toxic effects, a result that must be attributed to •OH quenching by NOM. Researchers have previously shown that NOM provides protection from •OH from irradiated TiO_2, but had not directly correlated changes in radical rate to toxicity (Wormington et al. 2017).

Recent literature has demonstrated that increased amounts of NOM and humic acid provide a protective effect against toxicity to *D. magna* (Wormington et al. 2017; Lüderwald et al. 2019) and to *Chlorella* sp. (Lin et al. 2012) resulting from TiO_2 NP irradiation. These studies also correlated increased NOM concentration to relative decreases in fluorescent equivalents. However, a direct correlation of toxicity to a reduction in quantitative radical concentration vis-à-vis the addition of NOM has yet to be established. Our work directly establishes radical generation rates for irradiated TiO_2 NP to toxicity based on the hydroxyl radical generation, and demonstrates reduction of these toxicity rates from the addition of NOM. We go on to link the reduction in toxicity as a result addition of NOM to a reduction in •OH generation rate, and show that more •OH are required to exert a similar toxic effect under conditions with high NOM compared to conditions with low NOM.

Broader Implications

These results directly quantify both radical accumulation and the attenuative effects of NOM that will allow for variations in regulatory actions regarding treatment and disposal of TiO_2 nanoparticles. The photocatalytic effects of TiO_2 nanoparticles are also leveraged for water treatment and breakdown of humic substances (Uyguner and Bekbolet 2005; Liu et al. 2010;

Drosos et al. 2015). Our results can aid in calculations for more efficient and more effective water treatments. The implications of TiO_2 NP interactions with NOM presented in this research also has relevancy considering worldwide climate change events. Drought-induced acidification of freshwater arboreal lakes results in DOC decreases sufficient enough to increase UV penetration depth by 3-fold (Yan et al. 1996). Increased amounts of TiO_2 nanoparticles in waters with less DOC can result in large-scale oxidative bursts, affecting the health of aquatic wildlife. Using the presented research, better long-term assessments can be made to incorporate the risk of TiO_2 nanoparticles entering an ever-changing aquatic environment.

CONCLUSIONS

In this work we demonstrate, under environmentally relevant conditions, that TiO_2 nanoparticles irradiated by simulated-sunlight generate both superoxide and hydroxyl radical species. We have quantitatively measured the change in radical production rates under changing conditions including addition of NOM and demonstrate that radical production rate heavily depends on a number of factors. Generation rate increases with increasing TiO_2 NP concentrations, and UV intensity, but is heavily attenuated by increasing amounts NOM. We provide arguments for describing produced radicals as $^{\bullet}OH$ to simplify toxicity estimations, while still including relevant radical species in our measurements.

Correlating TiO_2 NP toxicity as a function of $^{\bullet}OH$ provides a more accurate method of conservatively predicting toxicity compared to simply using TiO_2 nanoparticle concentration. TiO_2 NP alone are not toxic in the absence of UV-A light, exhibited by low *D. magna* mortality under no-UV or low UV conditions. Multiple radical species are detected in sunlight and sunlight like irradiated TiO_2 NP suspensions, but ultimately, $^{\bullet}OH$ is the species of greatest

concern. Therefore, measuring all generated species and modeling irradiated TiO_2-mediated ROS toxicity as $^{\bullet}OH$ gives upper bound $^{\bullet}OH$ values for LC50. Significantly higher $^{\bullet}OH$ production is required to induce similar *D. magna* mortality in suspensions with DOC, compared to suspensions without DOC. Thus, longer exposure periods, and/or higher TiO_2 NP concentrations in the system are required in DOC-containing samples for comparable toxicity. These results demonstrate the necessity of including both irradiant intensity, and DOC in toxicity measurements, as these factors are integral in assessing toxicity.

Supplemental Information: Supplemental information is available via the supplemental information files.

Data availability: Data, associated metadata, and calculation tools are available from the corresponding author (xxx)

Literature Cited

Al-Abed SR, Virkutyte J, Ortenzio JNR, McCarrick RM, Degn LL, Zucker R, Coates NH, Childs K, Ma H, Diamond S, et al. 2016. Environmental aging alters $Al(OH)_3$ coating of TiO_2 nanoparticles enhancing their photocatalytic and phototoxic activities. Environ Sci Nano. 3(3):593–601. doi:10.1039/c5en00250h.

Amiano I, Olabarrieta J, Vitorica J, Zorita S. 2012. Acute toxicity of nanosized TiO_2 to *Daphnia magna* under UVA irradiation. Environ Toxicol Chem. 31(11):2564–2566. doi:10.1002/etc.1981.

Ankley GT, Erickson RJ, Phipps GL, Mattson VR, Kosian PA, Sheedy BR, Cox JS. 1995. Effects of light intensity on the phototoxicity of fluoranthene to a benthic macroinvertebrate. Environ Sci Technol. 29(11):2828–2833. doi:10.1021/es00011a019.

Barron MG, Vivian D, Yee SH, Diamond SA. 2008. Temporal and spatial variation in solar radiation and photo-enhanced toxicity risks of spilled oil in Prince William Sound, Alaska, USA. Environ Toxicol Chem. 27(3):727–736. doi:10.1897/07-317.1.

Bosnjakovic A, Schlick S. 2006. Spin trapping by 5,5-dimethylpyrroline-N-oxide in fenton media in the presence of Nafion perfluorinated membranes: Limitations and potential. J Phys Chem B. 110(22):10720–10728. doi:10.1021/jp061042y.

631

632 Brezová V, Dvoranová D, Staško A. 2007. Characterization of titanium dioxide photoactivity
633 following the formation of radicals by EPR spectroscopy. Res Chem Intermed. 33(3–5):251–268.
634 doi:10.1163/156856707779238630.

635

636 Brunelli A, Pojana G, Callegaro S, Marcomini A. 2013. Agglomeration and sedimentation of
637 titanium dioxide nanoparticles (n-TiO_2) in synthetic and real waters. J Nanoparticle Res.
638 15(6):2711–2742. doi:10.1007/s11051-013-1684-4.

639

640 Bunsen R, Roscoe HE. 1862. Photochemische Untersuchungen. Ann Der Phys und Chemie. 12.

641

642 Cadet J, Davies KJA, Medeiros MH, Di Mascio P, Wagner JR. 2017. Formation and repair of
643 oxidatively generated damage in cellular DNA. Free Radic Biol Med. 107(December 2016):13–
644 34. doi:10.1016/j.freeradbiomed.2016.12.049.

645

646 Chen X, Mao SS. 2007. Titanium dioxide nanomaterials: Synthesis, properties, modifications,
647 and applications. Chem Rev. 107(7):2891–2959. doi:10.1021/cr0500535.

648

649 Číž M, Čížová H, Denev P, Kratchanova M, Slavov A, Lojek A. 2010. Different methods for
650 control and comparison of the antioxidant properties of vegetables. Food Control. 21(4):518–
651 523. doi:10.1016/j.foodcont.2009.07.017.

652

653 Cohn CA, Simon SR, Schoonen MAA. 2008. Comparison of fluorescence-based techniques for

the quantification of particle-induced hydroxyl radicals. Part Fibre Toxicol. 5:1–9. doi:10.1186/1743-8977-5-2.

Collin F. 2019. Chemical basis of reactive oxygen species reactivity and involvement in neurodegenerative diseases. Int J Mol Sci. 20(10). doi:10.3390/ijms20102407.

Cunningham J, Srijaranai S. 1988. Isotope-effect evidence for hydroxyl radical involvement in alcohol photo-oxidation sensitized by TiO2 in aqueous suspension. J Photochem Photobiol A Chem. 43(3):329–335. doi:10.1016/1010-6030(88)80029-7.

Diaz-Uribe CE, Daza MC, Martínez F, Páez-Mozo EA, Guedes CLB, Di Mauro E. 2010. Visible light superoxide radical anion generation by tetra(4-carboxyphenyl) porphyrin/TiO_2: EPR characterization. J Photochem Photobiol A Chem. 215(2–3):172–178. doi:10.1016/j.jphotochem.2010.08.013.

Diem S, von Rohr MR, Hering JG, Kohler H-PE, Schirmer M, von Gunten U. 2013. NOM degradation during river infiltration: Effects of the climate variables temperature and discharge. Water Res. 47(17):6585–6595. doi:10.1016/j.watres.2013.08.028.

Drosos M, Ren M, Frimmel FH. 2015. The effect of NOM to TiO_2: Interactions and photocatalytic behavior. Appl Catal B Environ. 165:328–334. doi:10.1016/j.apcatb.2014.10.017.

Dvoranová D, Barbieriková Z, Brezová V. 2014. Radical intermediates in photoinduced

reactions on TiO_2 (An EPR spin trapping study). Molecules. 19(11):17279–17304. doi:10.3390/molecules191117279.

Evans MD, Dizdaroglu M, Cooke MS. 2004. Oxidative DNA damage and disease: induction, repair and significance. Mutat Res Mutat Res. 567(1):1–61. doi:10.1016/j.mrrev.2003.11.001.

Forman HJ, Augusto O, Brigelius-Flohe R, Dennery PA, Kalyanaraman B, Ischiropoulos H, Mann GE, Radi R, Roberts LJ, Vina J, et al. 2015. Even free radicals should follow some rules: A Guide to free radical research terminology and methodology. Free Radic Biol Med. 78:233–235. doi:10.1016/j.freeradbiomed.2014.10.504.

Fu PP, Xia Q, Hwang HM, Ray PC, Yu H. 2014. Mechanisms of nanotoxicity: Generation of reactive oxygen species. J Food Drug Anal. 22(1):64–75. doi:10.1016/j.jfda.2014.01.005.

Fujishima A, Zhang X. 2006. Titanium dioxide photocatalysis: present situation and future approaches. Comptes Rendus Chim. 9(5–6):750–760. doi:10.1016/j.crci.2005.02.055.

Fujishima A, Zhang X, Tryk DA. 2008. TiO_2 photocatalysis and related surface phenomena. Surf Sci Rep. 63(12):515–582. doi:10.1016/j.surfrep.2008.10.001.

Gaigalas AK, Wang L, Cole KD, Humphries E. 2004. Photodegradation of fluorescein in solutions containing n-propyl gallate. J Phys Chem A. 108(20):4378–4384. doi:10.1021/jp0371377.

Gomes A, Fernandes E, Lima JLFC. 2005. Fluorescence probes used for detection of reactive oxygen species. J Biochem Biophys Methods. 65(2–3):45–80. doi:10.1016/j.jbbm.2005.10.003.

Goslan EH, Gurses F, Banks J, Parsons SA. 2006. An investigation into reservoir NOM reduction by UV photolysis and advanced oxidation processes. Chemosphere. 65(7):1113–1119. doi:10.1016/j.chemosphere.2006.04.041.

Gupta SM, Tripathi M. 2011. A review of TiO_2 nanoparticles. Chinese Sci Bull. 56(16):1639–1657. doi:10.1007/s11434-011-4476-1.

Harbour JR, Tromp J, Hair ML. 1985. Photogeneration of hydrogen peroxide in aqueous TiO_2 dispersions. Can J Chem. 63(1):204–208. doi:10.1139/v85-032.

Haynes VN, Ward JE, Russell BJ, Agrios AG. 2017. Photocatalytic effects of titanium dioxide nanoparticles on aquatic organisms − current knowledge and suggestions for future research. Aquat Toxicol.:1–38. doi:10.1016/j.aquatox.2017.02.012.

Hayyan M, Hashim MA, Alnashef IM. 2016. Superoxide Ion: Generation and Chemical Implications. Chem Rev. 116(5):3029–3085. doi:10.1021/acs.chemrev.5b00407.

He X, Sanders S, Aker WG, Lin Y, Douglas J, Hwang H. 2016. Assessing the effects of surface-bound humic acid on the phototoxicity of anatase and rutile TiO_2 nanoparticles in vitro. J

723 Environ Sci. 42(C):50–60. doi:10.1016/j.jes.2015.05.028.

724

725 Hirakawa T, Nosaka Y. 2002. Properties of $O_2^{\bullet-}$ and $^{\bullet}OH$ Formed in TiO_2 aqueous suspensions
726 by photocatalytic reaction and the influence of H2O2 and some ions. Langmuir. 18(8):3247–
727 3254. doi:10.1021/la015685a.

728

729 Huang X, Leal M, Li Q. 2008. Degradation of natural organic matter by TiO_2 photocatalytic
730 oxidation and its effect on fouling of low-pressure membranes. Water Res. 42(4–5):1142–1150.
731 doi:10.1016/j.watres.2007.08.030.

732

733 Ishibashi KI, Fujishima A, Watanabe T, Hashimoto K. 2000. Detection of active oxidative
734 species in TiO2 photocatalysis using the fluorescence technique. Electrochem commun.
735 2(3):207–210. doi:10.1016/S1388-2481(00)00006-0.

736

737 J.N.Junk M. 2012. Electron Paramagnetic Resonance theory. In: Assessing the functional
738 structure of molecular transporters by EPR spectroscopy. p. 7–52.

739

740 John R. Fowle III, Dearfield KL. 2006. Risk Characterization Handbook. (December):127.
741 Jovanović B. 2015. Review of titanium dioxide nanoparticle phototoxicity: Developing a
742 phototoxicity ratio to correct the endpoint values of toxicity tests. Environ Toxicol Chem.
743 34(5):1070–1077. doi:10.1002/etc.2891.

744

745 Keller AA, Lazareva A. 2013. Predicted Releases of Engineered Nanomaterials: From Global to

Regional to Local. Environ Sci Technol Lett. 1(1):65–70. doi:10.1021/ez400106t.

Keller AA, Wang H, Zhou D, Lenihan HS, Cherr G, Cardinale BJ, Miller R, Ji Z. 2010. Stability and aggregation of metal oxide nanoparticles in natural aqueous matrices. Environ Sci & Technol. 44(6):1962–1967. doi:10.1021/es902987d.

Kim J, Lee S, Kim C min, Seo J, Park Y, Kwon D, Lee SH, Yoon TH, Choi K. 2014. Non-monotonic concentration-response relationship of TiO_2 nanoparticles in freshwater cladocerans under environmentally relevant UV-A light. Ecotoxicol Environ Saf. 101(1):240–247. doi:10.1016/j.ecoenv.2014.01.002.

Klaine SJ, Alvarez PJJ, Batley GE, Fernandes TF, Handy RD, Lyon DY, Mahendra S, McLaughlin MJ, Lead JR. 2008. Nanomaterials in the environment: Behavior, fate, bioavailability, and effects. Environ Toxicol Chem. 27(9):1825. doi:10.1897/08-090.1.

Knorr FJ, Mercado CC, McHale JL. 2008. Trap-State distributions and carrier transport in pure and mixed-phase TiO_2: Influence of contacting solvent and interphasial electron transfer. J Phys Chem C. 112(33):12786–12794. doi:10.1021/jp8039934.

Konaka R, Kasahara E, Dunlap WC, Yamamoto Y, Chien KC, Inoue M. 2001. Ultraviolet irradiation of titanium dioxide in aqueous dispersion generates singlet oxygen. Redox Rep. 6(5):319–325. doi:10.1179/135100001101536463.

769 Lazareva A, Keller AA. 2014. Estimating potential life cycle releases of engineered
770 nanomaterials from wastewater treatment plants. ACS Sustain Chem Eng. 2(7):1656–1665.
771 doi:10.1021/sc500121w.
772
773 Li M, Yin JJ, Wamer WG, Lo YM. 2014. Mechanistic characterization of titanium dioxide
774 nanoparticle-induced toxicity using electron spin resonance. J Food Drug Anal. 22(1):76–85.
775 doi:10.1016/j.jfda.2014.01.006. http://dx.doi.org/10.1016/j.jfda.2014.01.006.
776
777 Li S, Erickson RJ, Wallis LK, Diamond SA, Hoff DJ. 2015. Modeling TiO_2 nanoparticle
778 phototoxicity: The importance of chemical concentration, ultraviolet radiation intensity, and
779 time. Environ Pollut. 205(C):327–332. doi:10.1016/j.envpol.2015.06.020.
780 Li S, Ma H, Wallis LK, Etterson MA, Riley B, Hoff DJ, Diamond SA. 2016. Impact of natural
781 organic matter on particle behavior and phototoxicity of titanium dioxide nanoparticles. Sci Total
782 Environ. 542:324–333. doi:10.1016/j.scitotenv.2015.09.141.
783
784 Lin D, Ji J, Long Z, Yang K, Wu F. 2012. The influence of dissolved and surface-bound humic
785 acid on the toxicity of TiO_2 nanoparticles to Chlorella sp. Water Res. 46(14):4477–4487.
786 doi:10.1016/j.watres.2012.05.035.
787
788 Liu S, Lim M, Fabris R, Chow C, Chiang K, Drikas M, Amal R. 2008. Removal of humic acid
789 using TiO_2 photocatalytic process – Fractionation and molecular weight characterisation studies.
790 Chemosphere. 72(2):263–271. doi:10.1016/j.chemosphere.2008.01.061.
791

Liu S, Lim M, Fabris R, Chow C, Drikas M, Amal R. 2010. Comparison of photocatalytic degradation of natural organic matter in two Australian surface waters using multiple analytical techniques. Org Geochem. 41(2):124–129. doi:10.1016/j.orggeochem.2009.08.008.

Loosli F, Le Coustumer P, Stoll S. 2013. TiO_2 nanoparticles aggregation and disaggregation in presence of alginate and Suwannee River humic acids. pH and concentration effects on nanoparticle stability. Water Res. 47(16):6052–6063. doi:10.1016/j.watres.2013.07.021.

Lüderwald S, Dackermann V, Seitz F, Adams E, Feckler A, Schilde C, Schulz R, Bundschuh M. 2019. A blessing in disguise? Natural organic matter reduces the UV light-induced toxicity of nanoparticulate titanium dioxide. Sci Total Environ. 663:518–526. doi:10.1016/j.scitotenv.2019.01.282.

Ma H, Brennan A, Diamond SA. 2012a. Photocatalytic reactive oxygen species production and phototoxicity of titanium dioxide nanoparticles are dependent on the solar ultraviolet radiation spectrum. Environ Toxicol Chem. 31(9):2099–2107. doi:10.1002/etc.1916.

Ma H, Brennan A, Diamond SA. 2012b. Phototoxicity of TiO_2 nanoparticles under solar radiation to two aquatic species: *Daphnia magna* and Japanese medaka. Environ Toxicol Chem. 31(7):1621–1629. doi:10.1002/etc.1858.

Mansfield CM, Alloy MM, Hamilton J, Verbeck GF, Newton K, Klaine SJ, Roberts AP. 2015. Photo-induced toxicity of titanium dioxide nanoparticles to *Daphnia magna* under natural

sunlight. Chemosphere. 120(C):206–210. doi:10.1016/j.chemosphere.2014.06.075.

Matilainen A, Sillanpää M. 2010. Removal of natural organic matter from drinking water by advanced oxidation processes. Chemosphere. 80(4):351–365. doi:10.1016/j.chemosphere.2010.04.067.

Miller RJ, Bennett S, Keller AA, Pease S, Lenihan HS. 2012. TiO_2 nanoparticles are phototoxic to marine phytoplankton. PLoS One. 7(1):e30321. doi:10.1371/journal.pone.0030321.

National Research Council. 1994. Science and Judgment in Risk Assessment. Washington, D.C.: National Academies Press. http://www.nap.edu/catalog/2125.

Newton GL, Milligan JR. 2006. Fluorescence detection of hydroxyl radicals. Radiat Phys Chem. 75(4):473–478. doi:10.1016/j.radphyschem.2005.10.011.

Nosaka Y, Komori S, Yawata K, Hirakawa T, Nosaka AY. 2003. Photocatalytic •OH radical formation in TiO2 aqueous suspension studied by several detection methods. Phys Chem Chem Phys. 5(20):4731–4735. doi:10.1039/b307433a.

Oris JT, Giesy JP. 1986. Photoinduced toxicity of anthracene to juvenile bluegill sunfish (*Lepomis Macrochirus rafinesque*): Photoperiod effects and predictive hazard evaluation. Environ Toxicol Chem. 5(8):761–768. doi:10.1002/etc.5620050807.

Ou B, Hampsch-Woodill M, Flanagan J, Deemer EK, Prior RL, Huang D. 2002. Novel

fluorometric assay for hydroxyl radical prevention capacity using fluorescein as the probe. J Agric Food Chem. 50(10):2772–2777. doi:10.1021/jf011480w.

Pelekani C, Newcombe G, Snoeyink VL, Hepplewhite C, Assemi S, Beckett R. 1999a. Characterization of natural organic matter using high performance size exclusion chromatography. Environ Sci Technol. 33(16):2807–2813. doi:10.1021/es9901314.

Pelekani C, Newcombe G, Snoeyink VL, Hepplewhite C, Assemi S, Beckett R. 1999b. Characterization of natural organic matter using high performance size exclusion chromatography. Environ Sci Technol. 33(16):2807–2813. doi:10.1021/es9901314.

Phaniendra A, Jestadi DB, Periyasamy L. 2015. Free radicals: Properties, sources, targets, and their implication in various diseases. Indian J Clin Biochem. 30(1):11–26. doi:10.1007/s12291-014-0446-0.

Praetorius A, Scheringer M, Hungerbühler K. 2012. Development of environmental fate models for engineered nanoparticles—A Case Study of TiO_2 nanoparticles in the Rhine River. Environ Sci & Technol. 46(12):6705–6713. doi:10.1021/es204530n.

Rao M V., Rajeshwar K, Pal Verneker VR, DuBow J. 1980. Photosynthetic production of H2 and H2O2 on semiconducting oxide grains in aqueous solutions. J Phys Chem. 84(15):1987–1991. doi:10.1021/j100452a023.

Robichaud CO, Uyar AE, Darby MR, Zucker LG, Wiesner MR. 2009. Estimates of upper bounds and trends in nano-TiO_2 production as a basis for exposure assessment. Environ Sci Technol. 43(12):4227–4233. doi:10.1021/es8032549.

Schneider J, Matsuoka M, Takeuchi M, Zhang J, Horiuchi Y, Anpo M, Bahnemann DW. 2014. Understanding TiO2 Photocatalysis: Mechanisms and Materials. Chem Rev. 114(19):9919–9986. doi:10.1021/cr5001892.

Scientific TF. 2010. Molecular Probes ™ Handbook. In: The Molecular Probes ® Handbook. 11th ed. p. 805–828. https://www.thermofisher.com/us/en/home/references/molecular-probes-the-handbook.html.

Sharma VK. 2009. Aggregation and toxicity of titanium dioxide nanoparticles in aquatic environment—A Review. J Environ Sci Heal Part A. 44(14):1485–1495. doi:10.1080/10934520903263231.

Shi H, Magaye R, Castranova V, Zhao J. 2013. Titanium dioxide nanoparticles: a review of current toxicological data. Part Fibre Toxicol. 10(1):15. doi:10.1186/1743-8977-10-15.

Shibata H, Ogura Y, Sawa Y, Kono Y. 1998. Hydroxyl radical generation depending on O_2 or H_2O by a photocatalyzed reaction in an aqueous suspension of titanium dioxide. Biosci Biotechnol Biochem. 62(12):2306–2311. doi:10.1271/bbb.62.2306.

Turchi CS, Ollis DF. 1990. Photocatalytic degradation of organic water contaminants:

Mechanisms involving hydroxyl radical attack. J Catal. 122(1):178–192. doi:10.1016/0021-9517(90)90269-p.

Uchino T, Tokunaga H, Ando M, Utsumi H. 2002. Quantitative determination of OH radical generation and its cytotoxicity induced by TiO_2–UVA treatment. Toxicol Vitr. 16(5):629–635. doi:10.1016/S0887-2333(02)00041-3.

United States Environmental Response Team. 1991. Compendium of ERT toxicity testing procedures: interim final. Washington, DC. http://nepis.epa.gov/Exe/ZyNET.exe/10001YL9.pdf.

USEPA. 2006. Whole Effluent Toxicity Training Video Series, Freshwater Series. (December). https://www.epa.gov/sites/production/files/2015-09/documents/wet_training.pdf.

Uyguner CS, Bekbolet M. 2005. Evaluation of humic acid photocatalytic degradation by UV–vis and fluorescence spectroscopy. Catal Today. 101(3–4):267–274. doi:10.1016/j.cattod.2005.03.011.

Wang GS, Hsieh ST, Hong CS. 2000. Destruction of humic acid in water by UV light - Catalyzed oxidation with hydrogen peroxide. Water Res. 34(15):3882–3887. doi:10.1016/S0043-1354(00)00120-2.

Wardman P. 2007. Fluorescent and luminescent probes for measurement of oxidative and nitrosative species in cells and tissues: Progress, pitfalls, and prospects. Free Radic Biol Med.

907 43(7):995–1022. doi:10.1016/j.freeradbiomed.2007.06.026.

908

909 Williamson CE. 1996. Effects of UV Radiation on freshwater ecosystems. Int J Environ Res

910 Public Health. 51:245–256.

911

912 Williamson CE, Stemberger RS, Morris DP, Frost TM, Paulsen SG. 1996. Ultraviolet radiation

913 in North American lakes: Attenuation estimates from DOC measurements and implications for

914 plankton communities. Limnol Oceanogr. 41(5):1024–1034. doi:10.4319/lo.1996.41.5.1024.

915

916 Wormington AM, Coral J, Alloy MM, Delmarè CL, Mansfield CM, Klaine SJ, Bisesi JH,

917 Roberts AP. 2017. Effect of natural organic matter on the photo-induced toxicity of titanium

918 dioxide nanoparticles. Environ Toxicol Chem. 36(6):1661–1666. doi:10.1002/etc.3702.

919

920 Wyrwoll AJ, Lautenschläger P, Bach A, Hellack B, Dybowska A, Kuhlbusch TAJ, Hollert H,

921 Schäffer A, Maes HM. 2016. Size matters - The phototoxicity of TiO_2 nanomaterials. Environ

922 Pollut. 208:859–867. doi:10.1016/j.envpol.2015.10.035.

923

924 Yan ND, Keller W, Scully NM, Lean DRS, Dillon PJ. 1996. Increased UV-B penetration in a

925 lake owing to drought-induced acidification. Nature. 381(6578):141–143. doi:10.1038/381141a0.

926

927 Yin J-J, Liu J, Ehrenshaft M, Roberts JE, Fu PP, Mason RP, Zhao B. 2012. Phototoxicity of nano

928 titanium dioxides in HaCaT keratinocytes—Generation of reactive oxygen species and cell

929 damage. Toxicol Appl Pharmacol. 263(1):81–88. doi:10.1016/j.taap.2012.06.001.

Zhang J, Nosaka Y. 2013. Quantitative detection of OH radicals for investigating the reaction mechanism of various visible-light TiO_2 Photocatalysts in aqueous suspension. J Phys Chem C. 117(3):1383–1391. doi:10.1021/jp3105166. https://pubs.acs.org/doi/10.1021/jp3105166.

Figure Captions:

Figure 1. **Spectra of ROS characterized by Electron Paramagnetic Resonance spectroscopy**. EPR characterization of radicals formed in simulated-sunlight irradiated TiO_2 NP suspensions. A) Copper sulfate, ascorbic acid, and hydrogen peroxide without irradiation generate hydroxyl radical resonances (Brezová et al. 2007; Diaz-Uribe et al. 2010; Dvoranová et al. 2014). B) TiO_2 nanoparticles under ultraviolet irradiation generate resonances for both hydroxyl (green) and superoxide (yellow) radicals, consistent with reported resonances for these species (Brezová et al. 2007; Miller et al. 2012; Dvoranová et al. 2014). DMPO (5,5-dimethyl-1-pyrroline-*N*-oxide) was used as a spin trap to generate both EPR spectra, and stars indicate formation of a nitroxide-like radical identified as a light-induced decomposition product of DMPO-$O_2^{\bullet-}$ (Bosnjakovic and Schlick 2006; Diaz-Uribe et al. 2010).

Figure 2. **ROS accumulation rates under simulated-sunlight irradiation.** Increasing concentrations of TiO_2 nanoparticle suspensions with increasing DOC concentrations under varying intensities of simulated sunlight to determine how varying conditions influence the rate accumulation of ROS. Simulated-sunlight irradiation intensities were 0 $\mu W/cm^2/nm$ (A), 2.671 $\mu W/cm^2/nm$ (B), 4.301 $\mu W/cm^2/nm$ (C), and 5.671 $\mu W/cm^2/nm$ (D). Radical generation rate was measured by fluorescence spectroscopy. Letters indicate level of significance; non-matching

letters are statistically significantly different within the TiO_2 treatment (α=0.05, $p < 0.05$), determined by one-way ANOVA, with a Tukey's HSD *post hoc* analysis to determine significantly different rates based on DOC concentration at a given intensity and TiO_2 NP concentration. Each *y*-axis has an increasing scale to better exhibit the differences in rate based on increasing DOC and TiO_2 concentrations under a given simulated-sunlight intensity. There were no significant differences in any of the 0 $\mu W/cm^2/nm$ data. Increases in ROS generation rate were well correlated to increased light intensity. Radical concentration rate was attenuated by increasing concentrations of DOC.

Figure 3. **48 h acute bioassays for *D. magna* toxicity to TiO_2 nanoparticles.** *Daphnia magna* LC50 toxicity to TiO_2 nanoparticles is dependent on the presence of UV light. *D manga* 48 h acute LC50 toxicity exposed to 0 $\mu W/cm^2/nm$ UV-A, 4.28 mg/L DOC: 837.0 (675.2, 1037.6) mg/L TiO_2 NPs; 4.301 $\mu W/cm^2/nm$ UV-A, 0 mg/L DOC: 0.156 (0.121, 0.199) mg/L TiO_2 NPs; 4.301 $\mu W/cm^2/nm$ UV-A, 4.28 mg DOC: 9.10 (8.37, 9.89) mg/L TiO_2 NPs.

Figure 4. **48 h acute bioassay for *D. magna* to hydroxyl radical.** *D. magna* toxicity described in terms of hydroxyl radical. TiO_2 nanoparticles generate radicals at an environmentally dependent rate. This rate is dependent on the interplay of UV intensity, DOC concentration, and TiO_2 nanoparticle concentration. *D. magna* LC50 toxicity for hydroxyl radical at 4.301 $\mu W/cm^2/nm$, 0 mg DOC: 0.458 (0.415, 0.503) μM $^{\bullet}OH$; 4.301 $\mu W/cm^2/nm$, 4.28 mg DOC: 6.216 (5.771, 6.691) μM $^{\bullet}OH$.

Figure 1.

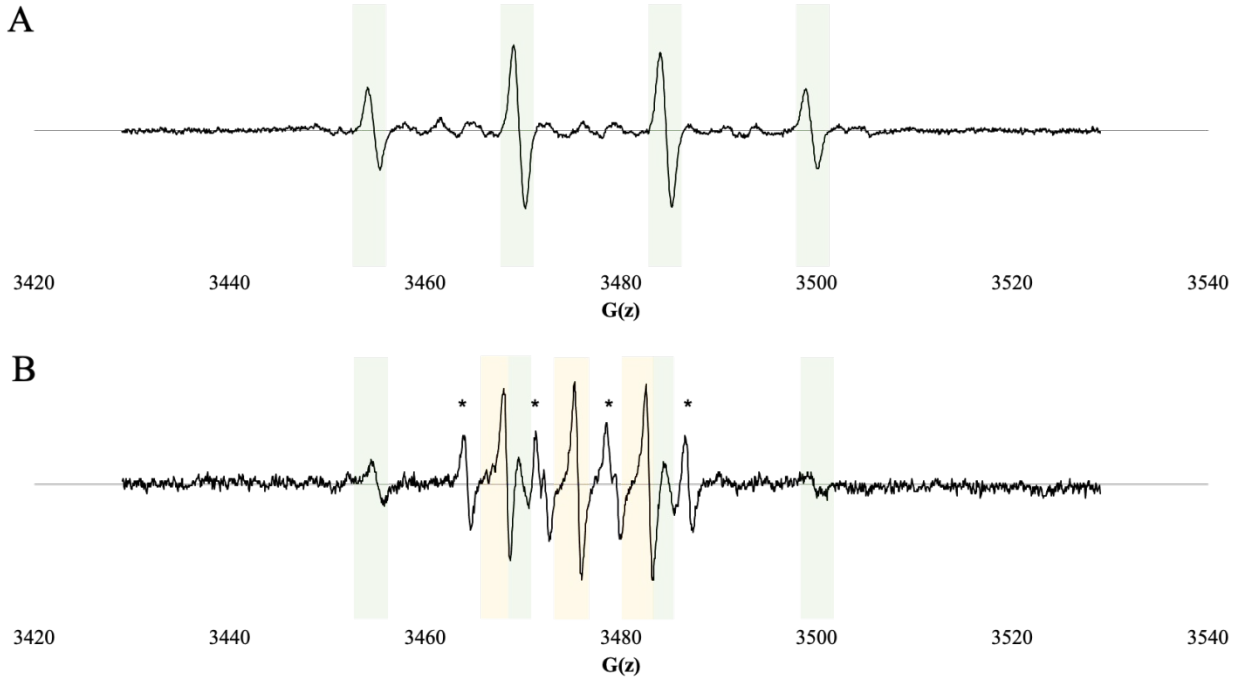
A
3420
3440
3460
3480
3500
3520
3540
G(z)
B
*
*
*
*
3420
3440
3460
3480
3500
3520
3540
G(z)

Figure 2.

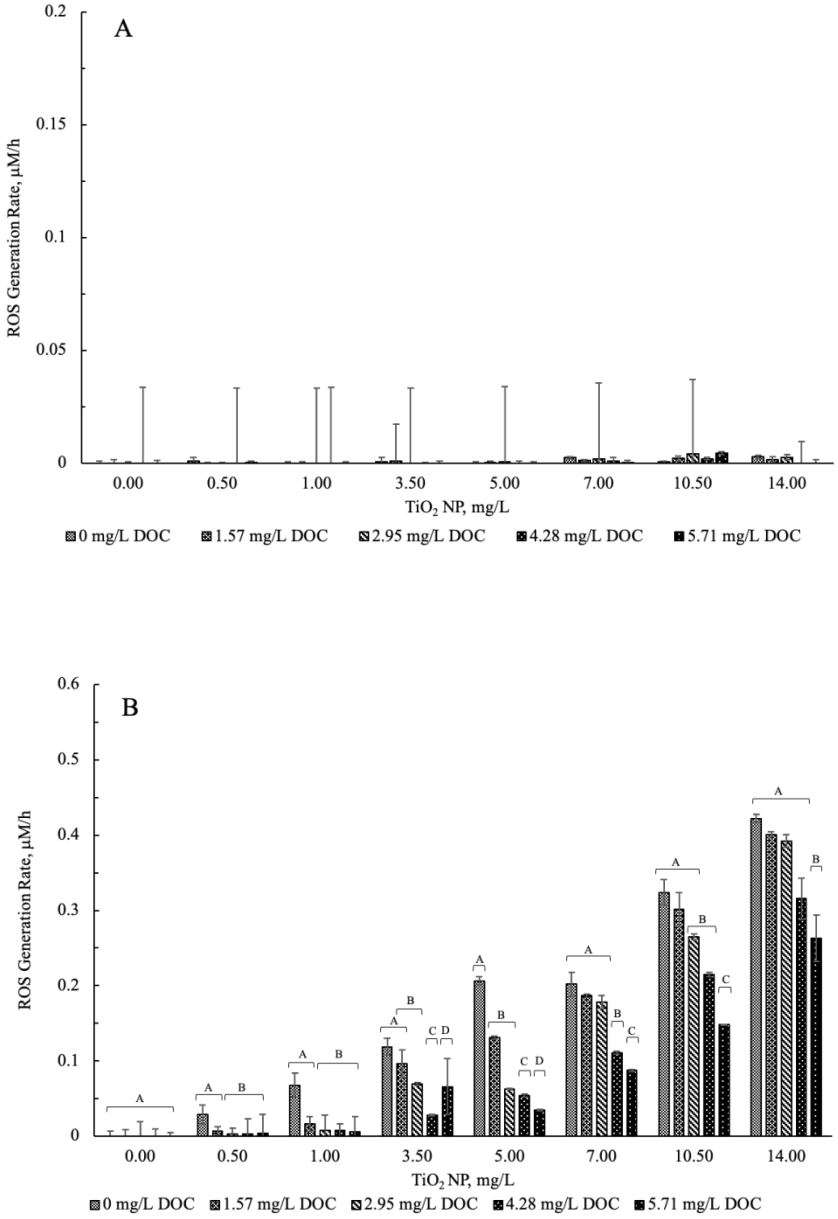
A
ROS Generation Rate, µM/h
0.2
0.15
0.1
0.05
0
0.00
0.50
1.00
3.50
5.00
7.00
10.50
14.00
TiO2 NP, mg/L
0 mg/L DOC
1.57 mg/L DOC
2.95 mg/L DOC
4.28 mg/L DOC
5.71 mg/L DOC
B
ROS Generation Rate, µM/h
0.6
0.5
0.4
0.3
0.2
0.1
0
TiO2 NP, mg/L
0 mg/L DOC
1.57 mg/L DOC
2.95 mg/L DOC
4.28 mg/L DOC
5.71 mg/L DOC

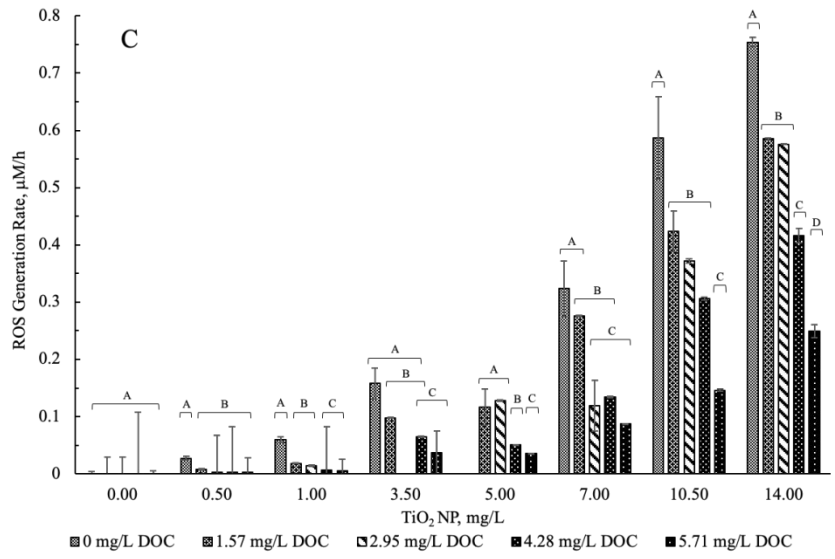
C
ROS Generation Rate, μM/h
0.8
0.7
0.6
0.5
0.4
0.3
0.2
0.1
0
0.00
0.50
1.00
3.50
5.00
7.00
10.50
14.00
TiO2 NP, mg/L
0 mg/L DOC
1.57 mg/L DOC
2.95 mg/L DOC
4.28 mg/L DOC
5.71 mg/L DOC

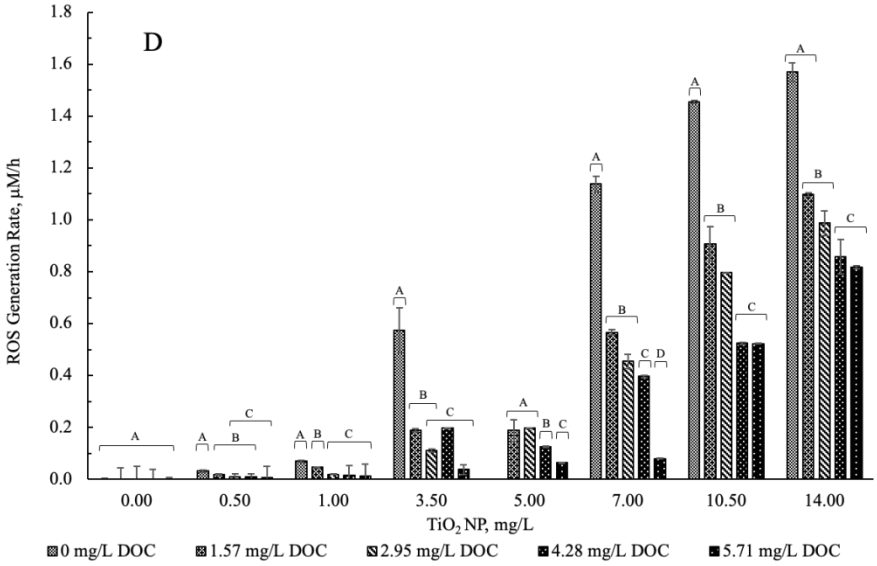
D
ROS Generation Rate, μM/h
1.8
1.6
1.4
1.2
1.0
0.8
0.6
0.4
0.2
0.0
0.00
0.50
1.00
3.50
5.00
7.00
10.50
14.00
TiO2 NP, mg/L
0 mg/L DOC
1.57 mg/L DOC
2.95 mg/L DOC
4.28 mg/L DOC
5.71 mg/L DOC

Figure 3.

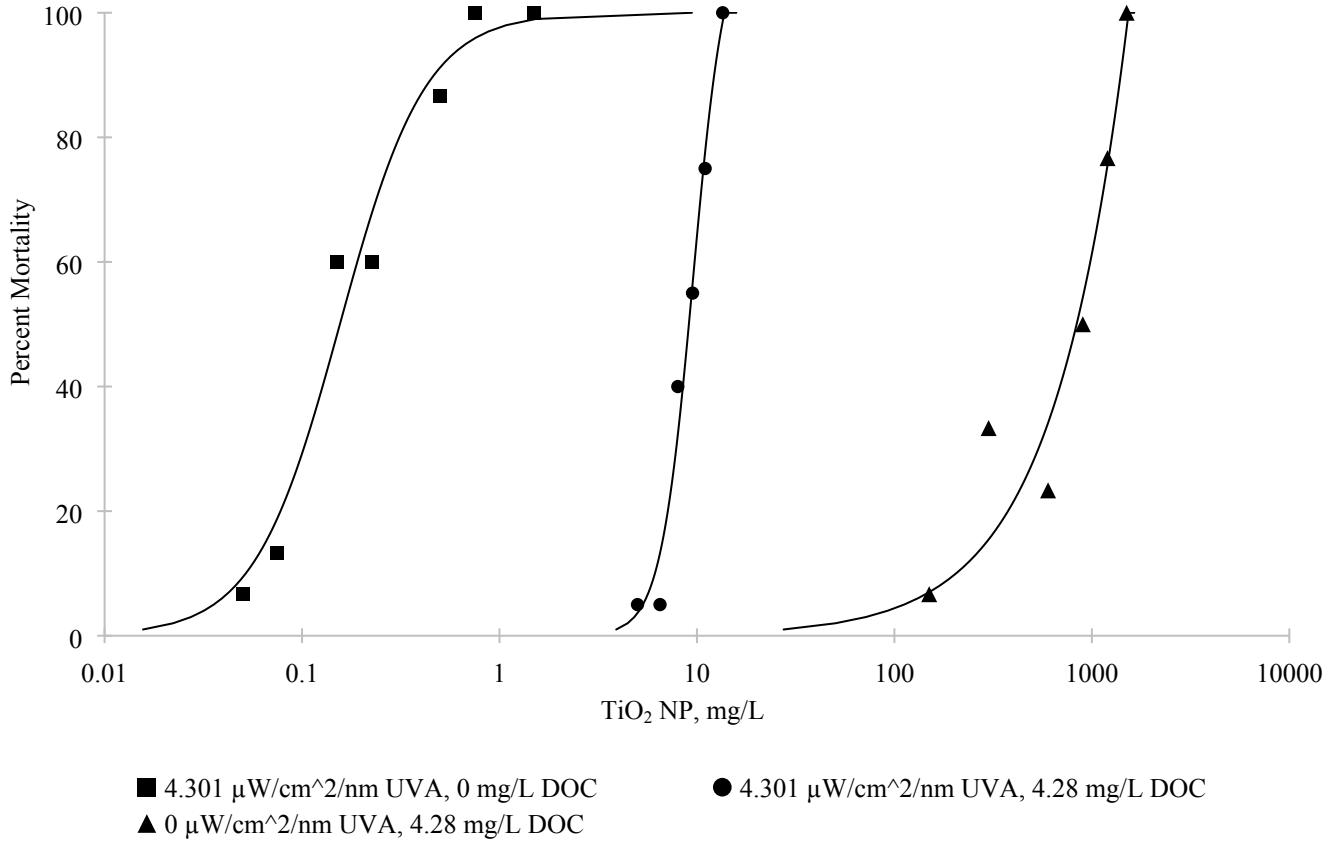
100
80
60
40
20
0
Percent Mortality
0.01
0.1
1
10
100
1000
10000
TiO2 NP, mg/L
4.301 µW/cm^2/nm UVA, 0 mg/L DOC
4.301 µW/cm^2/nm UVA, 4.28 mg/L DOC
0 µW/cm^2/nm UVA, 4.28 mg/L DOC

Figure 4.

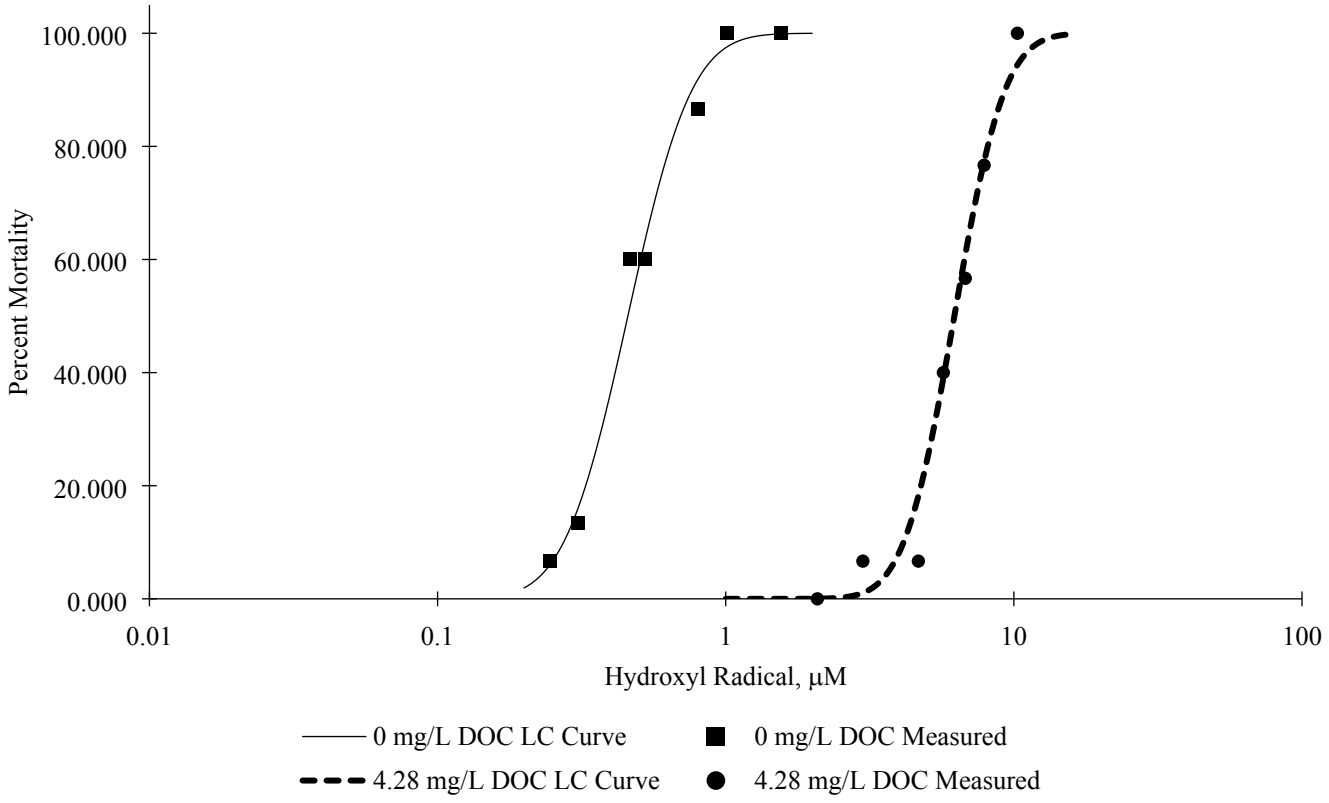
100.000
80.000
60.000
40.000
20.000
0.000
Percent Mortality
0.01
0.1
1
10
100
Hydroxyl Radical, µM
0 mg/L DOC LC Curve
0 mg/L DOC Measured
4.28 mg/L DOC LC Curve
4.28 mg/L DOC Measured